Available online at www.sciencedirect.com
SCIENCE DIRECT®
Journal of Sound and Vibration 286 (2005) 1001–1018
JOURNAL OF SOUND AND VIBRATION
www.elsevier.com/locate/jsvi

The crack effect on instability in a machine tool spindle with gas bearings

Bo-Wun Huang*

Department of Mechanical Engineering, Cheng Shiu University, No. 840 Cheng Ching Rd., Kaohsiung, Niaosung 833, Taiwan, ROC

Received 1 December 2003; received in revised form 27 June 2004; accepted 25 October 2004
Available online 24 December 2004

Abstract

Gas-bearing spindles are required for increased spindle speed in precise machining. Due to manufacturing flaws or cyclic loading, cracks frequently appear in a rotating spindle systems. Cracks markedly affect the dynamic characteristics of rotating machinery. Hence, in this study, high-speed spindles with gas bearings and the crack effect on the instability dynamics are considered. Most investigations on dynamic characteristics of the spindle system were confined to ball-bearing-type spindles. This work examines the dynamic instability in a cracked rotating spindle system with gas bearings. A round Euler–Bernoulli beam is used to approximate the spindle. The Hamilton principle is applied to derive the equation of motion for the spindle system. The effects of crack depth, rotation speed and provided air pressure on the dynamic instability of a rotating spindle system are studied

1. Introduction

During actual service, maintaining a constant spinning speed is nearly impossible because the spindle rotation is subjected to some small speed fluctuations. Theoretically, at a specific rotation speed, this small speed fluctuation may cause the system to become dynamically unstable, especially for a gas-bearing spindle. Most studies on spindle system instability were limited to the

*Fax: +886 7 7310213.
E-mail address: huangbw@csu.edu.tw (B.-W. Huang).

0022-460X/$ - see front matter © 2004 Elsevier Ltd. All rights reserved.
doi:10.1016/j.jsv.2004.10.029

spindle structure performance [1,2]. Only a few studies, such as Ref. [3], discussed the spindle stability with magnetic bearings. Accordingly, this study addresses the instability of a cracked rotating spindle with gas bearings.

Cracks, caused by manufacturing flaws or cyclic fatigue during operation, frequently appear in rotating machinery. In high-speed spindles, numerous cracks can be observed after severe operating conditions [4,5]. Local structural irregularities caused by cracks on the spindle may significantly change the dynamic behavior of a rotating machinery system. Many researchers have studied the crack effects on spindle system properties. The effects of cracks on the dynamic and static behaviors of structures have been studied in a number of papers [6–8]. More recent papers by Chen and Chen [9], Kuang and Huang [10] and Huang and Kuang [11] also dealt with investigations on rotating machinery with cracks. Some researchers [12–15] studied the effects of cracks on spindle, shaft and rotor system dynamics. In previous studies, the vibrational response of the rotating spindle was altered due to the crack opening and closing in one cycle when the spindle rotated. Most investigations were motivated by the thought that only a crack opening markedly changed the spindle dynamics. A spindle with a transverse crack is the focus of this study.

With the emergence of advanced cutting material technologies, it has become possible to adopt much higher cutting speeds than before. For a machining system, the spindle is the most critical element that affects the dynamic performance and capabilities in the machining process. In some investigations [16–19], the bearings could also change the dynamics of a machining spindle system. Hence, the bearing effects on the spindle system are studied in this article. Bearings are used in many rotating machines to brace the rotating spindles and rotors. In the past, the required rotor speed was sufficiently low allowing ball and roller bearings to be used in rotating machinery. High temperatures would be generated when ball-bearing spindle systems were operated at high speed. These high temperatures often brought about machining failure. Modern engineering technology allows greater complexity, accuracy, and rotating machinery that can attain high speeds. Non-contacting gas bearings are suitable for supporting a spindle and rotor in rotating machinery because of the high temperatures generated by the contact between the spindle and bearings.

Previous investigations on bearing spindle systems were confined to spindles with ball bearings. As in Refs. [16,17], the focus was on the dynamic response of a spindle supported by bearings and how the dynamics were influenced. At higher speeds, this bearing changed the stiffness of the entire spindle system and significantly altered the system properties, as described in Refs. [18–21]. Precise machining requires higher spindle speeds, making the gas-bearing spindle necessary. The performance and properties of gas bearings were examined in Refs. [22–26]. The application and design of gas bearings were discussed in Ref. [24].

Some investigations, as Refs. [27–29], on the dynamic characteristics of a cracked spindle system were confined to ball-bearing-type spindles. Few researchers paid attention to the dynamic instability of a cracked spindle system with gas bearings. The cracked gas-bearing spindle system is considered in this article. A round Euler–Bernoulli beam was used to approximate the spindle model. An actual-sized spindle is studied. The gas-bearing spindle is considered with massless springs used to model the bearing stiffness to simplify the calculations. The effects of crack depth, rotational speed and provided air pressure on the dynamic instability of a spindle system are investigated.

2. Equation of motion

This paper considers a spindle supported by gas bearings, as shown in Fig. 1(a) to elucidate the dynamic instability of a spindle system. Fig. 1(b) presents a simple model for this bearing–spindle system. In this model, a massless spring is employed to simulate the gas bearing stiffness. The spindle is supported by these springs. The rotational speed Ω must be considered in the rotating machinery. In this study, the deflection components $v(z,t)$ and $u(z,t)$ denote the two transverse flexible deflections of the spindle system. E and I represent the Young's Modulus and area inertial of the spindle, respectively.

The dimensionless governing equations of the spindle system are displayed as

$$\ddot{\bar{u}} - 2\sqrt{\frac{EI}{\rho AL^4}}\bar{\Omega}\dot{\bar{v}} + \frac{EI}{\rho AL^4}\left\{-\bar{\Omega}^2\bar{u} + (\bar{u}'')'' + \bar{k}_{x1}\bar{u}\delta(\bar{z}-\bar{z}_1) + \bar{k}_{x2}\bar{u}\delta(\bar{z}-\bar{z}_2)\right\} = 0, \tag{1}$$

$$\ddot{\bar{v}} + 2\sqrt{\frac{EI}{\rho AL^4}}\bar{\Omega}\dot{\bar{u}} + \frac{EI}{\rho AL^4}\left\{-\bar{\Omega}^2\bar{v} + (\bar{v}'')'' + \bar{k}_{y1}\bar{v}\delta(\bar{z}-\bar{z}_1) + \bar{k}_{y2}\bar{v}\delta(\bar{z}-\bar{z}_2)\right\} = 0, \tag{2}$$

where $\bar{k}_{x1}$ is the bearing stiffness in u deflection at a position $\bar{z}_1$, $\bar{k}_{y1}$ the bearing stiffness in v deflection at a position $\bar{z}_1$, $\bar{k}_{x2}$ the bearing stiffness in u deflection at a position $\bar{z}_2$, $\bar{k}_{y2}$ the bearing stiffness in v deflection at a position $\bar{z}_2$, and the dimensionless parameters are given by

$$\bar{z} = \frac{z}{L}, \quad \bar{z}_1 = \frac{z_1}{L}, \quad \bar{z}_2 = \frac{z_2}{L}, \quad \bar{\Omega} = \frac{\Omega}{\sqrt{EI/\rho AL^4}}, \tag{3}$$

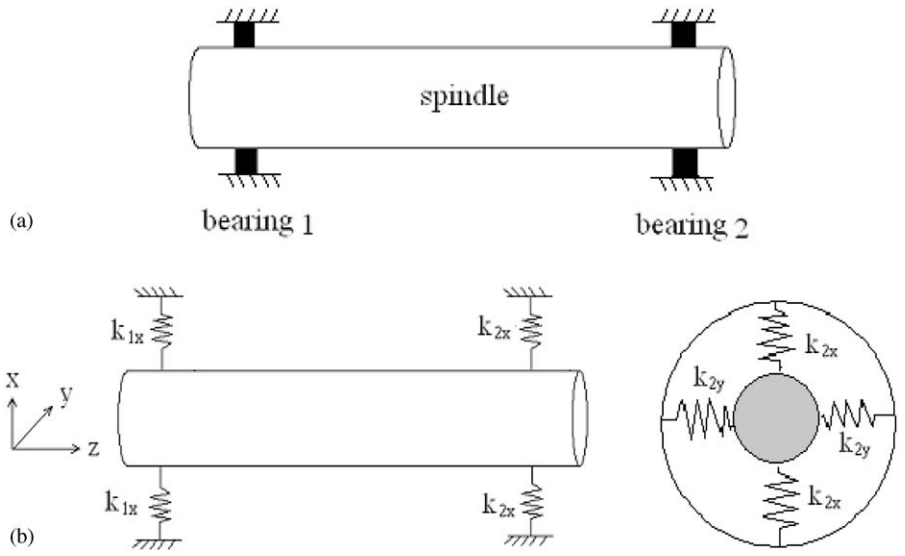

Fig. 1. A rotating spindle with bearings scheme. (a) a spindle supported by bearings, (b) a simple model of spindle–bearing systems.

$$\bar{u}(\bar{z}) = \frac{u(\bar{z})}{L}, \quad \bar{v}(\bar{z}) = \frac{v(\bar{z})}{L}, \quad \bar{k}_{x1} = \frac{k_{x1}L^3}{EI}, \quad \bar{k}_{x2} = \frac{k_{x2}L^3}{EI}, \tag{4}$$

$$\bar{k}_{y1} = \frac{k_{y1}L^3}{EI}, \quad \bar{k}_{y2} = \frac{k_{y2}L^3}{EI}, \tag{5}$$

and the boundary conditions are

$$\bar{u}'' = \bar{u}''' = \bar{v}'' = \bar{v}''' = 0 \quad \text{at } \bar{z} = 0, \tag{6}$$

$$\bar{u}'' = \bar{u}''' = \bar{v}'' = \bar{v}''' = 0 \quad \text{at } \bar{z} = 1. \tag{7}$$

The Galerkin method is employed to derive the equation of motion of the spindle, in matrix form. Therefore, the solutions of above equation can be assumed as

$$\bar{u}(\bar{z}, t) = \sum_{s=1}^{m} \phi_s(\bar{z}) p(t), \tag{8}$$

$$\bar{v}(\bar{z}, t) = \sum_{s=1}^{m} \varphi_s(\bar{z}) q(t), \tag{9}$$

where $\varphi_s(\bar{z})$, $\phi_s(\bar{z})$ are comparison functions for the spindle system, and $p(t)$, $q(t)$ are the coefficients to be determined about time for the system. The exact solution of the beam with free–free boundary conditions is considered, and five modes of comparison functions are used.

After complex calculations, the equations of motion, in matrix form, for the spindle system can be derived as

$$\begin{aligned}
&\begin{bmatrix} [M]_1 & 0 \\ 0 & [M]_2 \end{bmatrix} \begin{Bmatrix} \ddot{p}(t) \\ \ddot{q}(t) \end{Bmatrix} + 2\bar{\Omega}\alpha \begin{bmatrix} 0 & [G]_1 \\ [G]_2 & 0 \end{bmatrix} \begin{Bmatrix} \dot{p}(t) \\ \dot{q}(t) \end{Bmatrix} + \alpha^2 \begin{bmatrix} [K_e]_1 & 0 \\ 0 & [K_e]_2 \end{bmatrix} \begin{Bmatrix} p(t) \\ q(t) \end{Bmatrix} \\
&\quad + \bar{\Omega}^2\alpha^2 \begin{bmatrix} [K_\Omega]_1 & 0 \\ 0 & [K_\Omega]_2 \end{bmatrix} \begin{Bmatrix} p(t) \\ q(t) \end{Bmatrix} + \alpha^2 \begin{bmatrix} [K_{s1}]_1 & 0 \\ 0 & [K_{s1}]_2 \end{bmatrix} \begin{Bmatrix} p(t) \\ q(t) \end{Bmatrix} \\
&\quad + \alpha^2 \begin{bmatrix} [K_{s2}]_1 & 0 \\ 0 & [K_{s2}]_2 \end{bmatrix} \begin{Bmatrix} p(t) \\ q(t) \end{Bmatrix} = 0
\end{aligned} \tag{10}$$

where $\alpha = \sqrt{EI/\rho AL^4}$. The elements of the matrix in the above equation are given as follows:

$$(m_{ij})_1 = \int_0^1 \phi_i \phi_j \, \mathrm{d}\bar{z} = -[(k_\Omega)_{ij}]_1, \tag{11}$$

$$(m_{ij})_2 = \int_0^1 \varphi_i \varphi_j \, \mathrm{d}\bar{z} = -[(k_\Omega)_{ij}]_2, \tag{12}$$

$$(g_{ij})_1 = -\int_0^1 \phi_i \varphi_j \, \mathrm{d}\bar{z}, \tag{13}$$

$$(g_{ij})_2 = \int_0^1 \varphi_i \phi_j \, \mathrm{d}\bar{z}, \tag{14}$$

$$[(k_e)_{ij}]_1 = \int_0^1 \phi_i'' \phi_j'' \, \mathrm{d}\bar{z}, \tag{15}$$

$$[(k_e)_{ij}]_2 = \int_0^1 \varphi_i'' \varphi_j'' \, \mathrm{d}\bar{z}, \tag{16}$$

$$[(k_{s1})_{ij}]_1 = \bar{k}_{x1}\{\phi_i(\bar{z}_1)\}\{\phi_j(\bar{z}_1)\}^{\mathrm{T}}, \tag{17}$$

$$[(k_{s1})_{ij}]_2 = \bar{k}_{y1}\{\varphi_i(\bar{z}_1)\}\{\varphi_j(\bar{z}_1)\}^{\mathrm{T}}, \tag{18}$$

$$[(k_{s2})_{ij}]_1 = \bar{k}_{x2}\{\phi_i(\bar{z}_2)\}\{\phi_j(\bar{z}_2)\}^{\mathrm{T}}, \tag{19}$$

$$[(k_{s2})_{ij}]_2 = \bar{k}_{y2}\{\varphi_i(\bar{z}_2)\}\{\varphi_j(\bar{z}_2)\}^{\mathrm{T}}. \tag{20}$$

The rotational speed is assumed to be fluctuated with a small perturbation speed $\bar{f}(t)$, and can be written as

$$\bar{\Omega}(t) = \bar{\Omega}_0 + \bar{f}(t), \tag{21}$$

where $\bar{\Omega}_0 = \Omega_0/\sqrt{EI/\rho AL^4}$ and $\bar{f}(t) = f(t)/\sqrt{EI/\rho AL^4}$.

The governing equations are rewritten as

$$\begin{aligned}
&\begin{bmatrix} [M]_1 & 0 \\ 0 & [M]_2 \end{bmatrix} \begin{Bmatrix} \ddot{p}(t) \\ \ddot{q}(t) \end{Bmatrix} + 2\bar{\Omega}_0\alpha \begin{bmatrix} 0 & [G]_1 \\ [G]_2 & 0 \end{bmatrix} \begin{Bmatrix} \dot{p}(t) \\ \dot{q}(t) \end{Bmatrix} + \alpha^2 \begin{bmatrix} [K_e]_1 & 0 \\ 0 & [K_e]_2 \end{bmatrix} \begin{Bmatrix} p(t) \\ q(t) \end{Bmatrix} \\
&\bar{\Omega}_0^2\alpha^2 \begin{bmatrix} [K_\Omega]_1 & 0 \\ 0 & [K_\Omega]_2 \end{bmatrix} \begin{Bmatrix} p(t) \\ q(t) \end{Bmatrix} + \alpha^2 \begin{bmatrix} [K_{s1}]_1 & 0 \\ 0 & [K_{s1}]_2 \end{bmatrix} \begin{Bmatrix} p(t) \\ q(t) \end{Bmatrix} + \alpha^2 \begin{bmatrix} [K_{s2}]_1 & 0 \\ 0 & [K_{s2}]_2 \end{bmatrix} \begin{Bmatrix} p(t) \\ q(t) \end{Bmatrix} \\
&= 2\left(\bar{f}\dot{\bar{\Omega}}_0 + \bar{f}^2\right)\alpha^2 \begin{bmatrix} -[K_\Omega]_1 & 0 \\ 0 & -[K_\Omega]_2 \end{bmatrix} \begin{Bmatrix} p(t) \\ q(t) \end{Bmatrix} + 2\bar{f}\alpha \begin{bmatrix} -[G]_1 & 0 \\ 0 & -[G]_2 \end{bmatrix} \begin{Bmatrix} \dot{p}(t) \\ \dot{q}(t) \end{Bmatrix}.
\end{aligned} \tag{22}$$

Therefore, Eq. (22) can be re-displayed as

$$[M]\{\ddot{X}\} + \alpha[G]\{\dot{X}\} + \alpha^2[K]\{X\} = 2\alpha\bar{f}[D]\{\dot{X}\} + \alpha^2\left(2\bar{\Omega}_0\bar{f} + \bar{f}^2\right)[E]\{X\}. \tag{23}$$

A space vector is introduced in Eq. (23) to solve the eigenvalue problem of the system:

$$\{V\} = \begin{Bmatrix} \dot{X} \\ X \end{Bmatrix}. \tag{24}$$

Substituting Eq. (24) into Eq. (23), the equation can be rearranged as

$$\begin{bmatrix} [M] & 0 \\ 0 & \alpha^2[K] \end{bmatrix} \{\dot{V}\} + \begin{bmatrix} \alpha[G] & \alpha^2[K] \\ -\alpha^2[K] & 0 \end{bmatrix} \{V\} = 2\bar{f} \begin{bmatrix} \alpha[D] & 0 \\ 0 & 0 \end{bmatrix} \{V\} + \left(2\bar{\Omega}_0 \bar{f} + f^2\right) \begin{bmatrix} 0 & \alpha^2[E] \\ 0 & 0 \end{bmatrix} \{V\}. \tag{25}$$

The non-dimensional frequency $\bar{\omega}_n$ in Eq. (25), i.e., the natural frequency of the spindle system, is defined as

$$\bar{\omega}_n = \omega_n \Big/ \sqrt{\frac{EI}{\rho A L^4}} \qquad \text{for } n = 1, 2, \ldots \tag{26}$$

2.1. Crack effect

Considering a crack located at $\bar{z} = \bar{z}^*$ on this spindle, the strain energy of the defective spindle will include the released energy caused by the crack. Fig. 2 shows the geometry of a cracked spindle. The released energy caused by a crack, as noted in Ref. [30], with a depth of a may be expressed as

$$U^c = \int_{-b}^{b} \frac{(1-\mu^2)}{E} K_I^2(\xi)\, \mathrm{d}\xi, \tag{27}$$

where $b = \sqrt{R^2 - (R-a)^2}$.

μ is the Poisson's ratio of the spindle, K_I is the stress intensity factor under a mode I load and R is the radius of the spindle. This stress intensity factor K_I will be considered. In this case, the stress intensity factors K_I can be approximated as

$$K_I(\xi) = \frac{4P_b}{\pi R^4} \sqrt{R^2 - \xi^2} \sqrt{\pi\alpha}\, F_2\left(\frac{\alpha}{h}\right), \tag{28}$$

where P_b is the a bending moment, and

$$h = 2\sqrt{R^2 - \xi^2}, \tag{29}$$

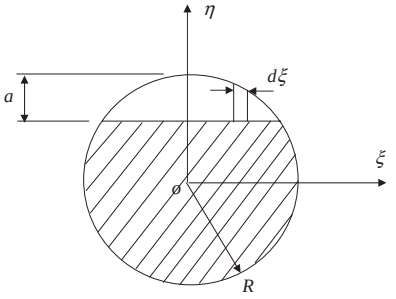

Fig. 2. Geometry of a crack spindle.

$$\alpha = a + \sqrt{R^2 - \xi^2} - R, \tag{30}$$

$$F_2\left(\frac{\alpha}{h}\right) = \sqrt{\frac{2h}{\pi\alpha}\tan\left(\frac{\pi\alpha}{2h}\right)}\,\frac{0.923 + 0.199[1 - \sin(\pi\alpha/2h)]^4}{\cos(\pi\alpha/2h)}. \tag{31}$$

The notations a and R are the maximum crack depth and radius of the spindle, respectively. Based on the investigations in Refs. [30,31], alterations in the elastic deformation energy caused by lateral bending moments are the only important change in the case of slender beams with a crack. Due to the bending moment, the released energy by the crack with respect to ξ is obtained as

$$U_{\xi}^{c} = E(1-\mu^2)\pi \int_0^L \int_0^a \int_{-b}^{b} \left[\frac{\partial^2 v}{\partial z^2}\,\delta(z - z^*)\right]^2 (R^2 - \xi^2)\alpha F_2^2\left(\frac{\alpha}{h}\right) \mathrm{d}\xi\,\mathrm{d}\alpha\,\mathrm{d}z. \tag{32}$$

Similarly, the released energy by the crack with respect to η is derived as follows:

$$U_{\eta}^{c} = E(1-\mu^2)\pi \int_0^L \int_0^a \int_{-b}^{b} \left[\frac{\partial^2 u}{\partial z^2}\,\delta(z - z^*)\right]^2 \xi^2 \alpha F_1^2\left(\frac{\alpha}{h}\right) \mathrm{d}\xi\,\mathrm{d}\alpha\,\mathrm{d}z, \tag{33}$$

where

$$F_1\left(\frac{\alpha}{h}\right) = \sqrt{\frac{2h}{\pi\alpha}\tan\left(\frac{\pi\alpha}{2h}\right)}\,\frac{0.752 + 2.02(\alpha/h) + 0.37[1 - \sin(\pi\alpha/2h)]^3}{\cos(\pi\alpha/2h)}. \tag{34}$$

To simplify, the flexibility coefficients, the dimensionless equations, as functions of crack depth a/R for a circular are employed as

$$U_{\eta}^{c} = \frac{4R}{L}(1-\mu^2)\pi \int_0^1 \left[\frac{\partial^2 \bar{u}}{\partial \bar{z}^2}\,\delta(\bar{z} - \bar{z}^*)\right]^2 Q_1\left(\frac{\xi}{R}, \frac{\alpha}{R}\right) \mathrm{d}\bar{z}, \tag{35}$$

$$U_{\xi}^{c} = \frac{4R}{L}(1-\mu^2)\pi \int_0^1 \left[\frac{\partial^2 \bar{v}}{\partial \bar{z}^2}\,\delta(\bar{z} - \bar{z}^*)\right]^2 Q_2\left(\frac{\xi}{R}, \frac{\alpha}{R}\right) \mathrm{d}\bar{z}, \tag{36}$$

where

$$Q_1\left(\frac{\xi}{R}, \frac{\alpha}{R}\right) = \int_0^{a/R} \int_{-b/R}^{b/R} \frac{\xi^2}{R^2}\,\frac{\alpha}{R}\,F_1^2\left(\frac{\alpha}{h}\right) \mathrm{d}\,\frac{\xi}{R}\,\mathrm{d}\,\frac{\alpha}{R}, \tag{37}$$

$$Q_2\left(\frac{\xi}{R}, \frac{\alpha}{R}\right) = \int_0^{a/R} \int_{-b/R}^{b/R} \left(1 - \frac{\xi^2}{R^2}\right)\frac{\alpha}{R}\,F_2^2\left(\frac{\alpha}{h}\right) \mathrm{d}\,\frac{\xi}{R}\,\mathrm{d}\,\frac{\alpha}{R}. \tag{38}$$

The bearing–spindle with a crack can then be obtained as

$$\ddot{\bar{u}} - 2\sqrt{\frac{EI}{\rho A L^4}}\,\bar{\Omega}\dot{\bar{v}} + \frac{EI}{\rho A L^4}\left\{-\bar{\Omega}^2\bar{u} + (\bar{u}'')'' - \frac{8R}{L}(1-\mu^2)Q_1\left(\frac{\xi}{R}, \frac{\alpha}{R}\right)[\bar{u}''\delta(\bar{z} - \bar{z}^*)]'' + \bar{k}_{x1}\bar{u}\delta(\bar{z} - \bar{z}_1) + \bar{k}_{x2}\bar{u}\delta(\bar{z} - \bar{z}_2)\right\} = 0, \tag{39}$$

$$\ddot{\bar{v}} + 2\sqrt{\frac{EI}{\rho AL^4}}\bar{\Omega}\dot{\bar{u}} + \frac{EI}{\rho AL^4}\left\{-\bar{\Omega}^2\bar{v} + (\bar{v}'')'' - \frac{8R}{L}(1-\mu^2)Q_2\left(\frac{\xi}{R},\frac{\alpha}{R}\right)[\bar{v}''\delta(\bar{z}-\bar{z}^*)]'' \right.$$
$$\left. \bar{k}_{y1}\bar{v}\delta(\bar{z}-\bar{z}_1) + \bar{k}_{y2}\bar{v}\delta(\bar{z}-\bar{z}_2)\right\} = 0. \tag{40}$$

2.2. Supported by gas bearing

Many engineering applications for spindle systems must depend on gas bearings at high speed, low temperature and under light cutting conditions. Hence, ball bearings are no longer suitable for broad use. Gas bearings have frequently been used to support high-speed spindles, especially for printed circuit board (PCB) drilling. In this investigation, the dynamic instability of a spindle with a gas bearing is of interest. As in Ref. [24], the stiffness of the gas bearing is given by

$$k_g = \frac{\mathrm{d}\,W}{\mathrm{d}\,h}, \tag{41}$$

where W is the work caused by lubricant pressure and h is the clearance for the gas bearing. As above, the stiffness of the gas bearing can be displayed as

$$k_g = \frac{(p_s - p_a)L_g D_g}{C_g}\bar{k}_g, \tag{42}$$

where C_g is the radius clearance for the bearing, L_g the bearing length, D_g the bearing diameter, P_s the provided pressure, P_a the atmospheric pressure and

$$\bar{k}_g = \frac{W}{e(p_s - p_a)L_g D_g}, \tag{43}$$

where e is the eccentric ratio of the bearing. As stated above, the non-dimensional gas bearing stiffness, $\bar{k}_g$, can be found if the applied air coefficient Γ_s and the eccentric ratio of the bearing, e, are known. Furthermore, the bearing radius clearance, C_g, is derived as

$$C_g = \left(\frac{24\mu n d_g\sqrt{gRT_0}}{p_s\Gamma_s}\frac{L_g}{D_g}\right)^{1/2}, \tag{44}$$

where $\mu = 1.833\times10^{-10}\,\mathrm{kg\,s/cm^2}$ is the viscosity, $n = 8$ is the number of pores, $d_g = 0.05\,\mathrm{mm}$ is the pore diameter, g the gravity acceleration, R the gas constant, and T_0 the temperature.

3. Perturbation analysis

The equation of motion, as above, is a set of simultaneous differential equation, which cannot be investigated directly in this study. Modal analysis is employed to make the calculation even easier. For brevity, displacement vector $\{V\}$ is defined as $[\Delta]\{u\}$, where $[\Delta]$ is the modal matrix and is composed of the real and imaginary eigenvectors of this system. After this modal analysis, the

simultaneous different equation is rewritten as

$$[I]\{\dot{u}\} + [A]\{u\} = -2\frac{\bar{f}}{\bar{\Omega}_0}[S]\{u\} - \left(\frac{2\bar{f}}{\bar{\Omega}_0} + \frac{\bar{f}^2}{\bar{\Omega}_0^2}\right)[Q]\{u\}, \tag{45}$$

where $[I]$ is a unit matrix. Eq. (45) can then be decoupled and written in component form as

$$\dot{\varsigma}_n - \bar{\omega}_n\eta_n = -2\frac{\bar{f}}{\bar{\Omega}_0}\left(\sum_{r=1}^{R} S_{nr}^{11}\zeta_r + \sum_{r=1}^{R} S_{nr}^{12}\eta_r\right) - \left(2\frac{\bar{f}}{\bar{\Omega}_0} + \frac{\bar{f}^2}{\bar{\Omega}_0^2}\right)\left(\sum_{r=1}^{R} Q_{nr}^{11}\zeta_r + \sum_{r=1}^{R} Q_{nr}^{12}\eta_r\right), \tag{46}$$

$$\dot{\eta}_n + \bar{\omega}_n\varsigma_n = -2\frac{\bar{f}}{\bar{\Omega}_0}\left(\sum_{r=1}^{R} S_{nr}^{21}\zeta_r + \sum_{r=1}^{R} S_{nr}^{22}\eta_r\right) - \left(2\frac{\bar{f}}{\bar{\Omega}_0} + \frac{\bar{f}^2}{\bar{\Omega}_0^2}\right)\left(\sum_{r=1}^{R} Q_{nr}^{21}\zeta_r + \sum_{r=1}^{R} Q_{nr}^{22}\eta_r\right), \tag{47}$$

where S_{nl}^{ij} and Q_{nl}^{ij} are the i–jth entries for the n–lth block matrices of $[S]$ and $[Q]$ and $\{u\} = [\varsigma_1, \eta_1, \varsigma_2, \eta_2, \ldots, \varsigma_R, \eta_R]$.

The perturbation velocity, $\bar{f}(t)$, is assumed to be small and periodic. Therefore, it can be expanded as a Fourier series, $\bar{f}(t) = \sum_{j=-Q}^{Q} F_j e^{i\bar{\omega}_j t}$, where the parameter $\bar{\omega}_j$ is the perturbation frequency. As noted, the fluctuation term $\bar{f}(t)$ is very small in comparison to the constant speed $\bar{\Omega}_0$; so, the module F_j is much smaller than $\bar{\Omega}_0$. Consider a small parameter term, ε, defined as $|F_M|/\bar{\Omega}_0$, where $|F_M|$ is the maximum magnitude of components F_j for $j = 1, 2, 3, \ldots, Q$. Eqs. (46) and (47) can then be rewritten as

$$\dot{\varsigma}_n - \bar{\omega}_n\eta_n = -2\varepsilon\tilde{f}\left(\sum_{r=1}^{R} S_{nr}^{11}\zeta_r + \sum_{r=1}^{R} S_{nr}^{12}\eta_r\right) - \left(2\varepsilon\tilde{f} + \varepsilon^2\tilde{f}^2\right)\left(\sum_{r=1}^{R} Q_{nr}^{11}\zeta_r + \sum_{r=1}^{R} Q_{nr}^{12}\eta_r\right), \tag{48}$$

$$\dot{\eta}_n + \bar{\omega}_n\varsigma_n = -2\varepsilon\tilde{f}\left(\sum_{r=1}^{R} S_{nr}^{21}\zeta_r + \sum_{r=1}^{R} S_{nr}^{22}\eta_r\right) - \left(2\varepsilon\tilde{f} + \varepsilon^2\tilde{f}^2\right)\left(\sum_{r=1}^{R} Q_{nr}^{21}\zeta_r + \sum_{r=1}^{R} Q_{nr}^{22}\eta_r\right), \tag{49}$$

where $\tilde{f} = \bar{f}/|F_M|$.

By employing the multiple scales perturbation method [32], the solution for Eqs. (48) and (49) can then be expressed in terms as

$$u_n(t,\varepsilon) = u_{n0}(T_0, T_1, T_2, \ldots) + \varepsilon u_{n1}(T_0, T_1, T_2, \ldots) + \varepsilon^2 u_{n2}(T_0, T_1, T_2, \ldots) + \cdots \tag{50}$$

where $T_\alpha = \varepsilon^\alpha t$ for $\alpha = 0, 1, 2, \ldots$.

Substituting Eq. (48) into Eqs. (46) and (47), yields

$$\text{order } \varepsilon^0 \quad D_0\varsigma_{n0} - \bar{\omega}_n\eta_{n0} = 0, \tag{51}$$

$$D_0\eta_{n0} + \bar{\omega}_n\varsigma_{n0} = 0, \tag{52}$$

$$\text{order } \varepsilon^1 \qquad D_0\varsigma_{n1} - \bar{\omega}_n\eta_{n1} = -D_1\varsigma_{n0} - 2\tilde{f}\left(\sum_{r=1}^{R} S_{nr}^{11}\zeta_{r0} + \sum_{r=1}^{R} S_{nr}^{12}\eta_{r0}\right) - 2\tilde{f}\left(\sum_{r=1}^{R} Q_{nr}^{11}\zeta_{r0} + \sum_{r=1}^{R} Q_{nr}^{12}\eta_{r0}\right), \tag{53}$$

$$D_0\eta_{n1} + \bar{\omega}_n\varsigma_{n1} = -D_1\eta_{n0} - 2\tilde{f}\left(\sum_{r=1}^{R} S_{nr}^{21}\zeta_{r0} + \sum_{r=1}^{R} S_{nr}^{22}\eta_{r0}\right) - 2\tilde{f}\left(\sum_{r=1}^{R} Q_{nr}^{21}\zeta_{r0} + \sum_{l=1}^{R} Q_{nr}^{22}\eta_{r0}\right), \tag{54}$$

where

$$\frac{\mathrm{d}}{\mathrm{d}t} = \frac{\mathrm{d}T_0}{\mathrm{d}t}\frac{\partial}{\partial T_0} + \frac{\mathrm{d}T_1}{\mathrm{d}t}\frac{\partial}{\partial T_1} + \frac{\mathrm{d}T_2}{\mathrm{d}t}\frac{\partial}{\partial T_2}\cdots = D_0 + \varepsilon D_1 + \varepsilon^2 D_2\cdots \tag{55}$$

and $\partial/\partial T_j = D_j$.

The second-order expansion is not performed because of the complexity of this investigation and the slight difference between the results from the first- and second-order approximations [33–35]. The first-order approximate solution is

$$\varsigma_{n0} = A_n(T_1)\exp(\mathrm{i}\bar{\omega}_n T_0) + \text{c.c.}, \tag{56}$$

$$\eta_{n0} = \mathrm{i}A_n(T_1)\exp(\mathrm{i}\bar{\omega}_n T_0) + \text{c.c.}, \tag{57}$$

where $A_n(T_1)$ is an undetermined function of T_1, and the corresponding complex conjugate terms are denoted by c.c.. Assuming that $\tilde{f}_0 = 0$ and $\tilde{f} = \sum_{j=1}^{Q}\hat{F}_k\mathrm{e}^{\mathrm{i}\omega_j t} + \text{c.c.}$, and substituting the general solutions, Eqs. (56) and (57) into Eqs. (53) and (54), yields the following solutions:

$$\begin{aligned} D_0\varsigma_{n1} - \bar{\omega}_n\eta_{n1} = {} & D_1 A_n \mathrm{e}^{\mathrm{i}\bar{\omega}_n T_0} \\ & - 2\sum_{j=1}^{Q}\hat{F}_j\sum_{r=1}^{R} S_{nr}^{11}\left\{A_r\mathrm{e}^{\mathrm{i}[\bar{\omega}_j+\bar{\omega}_r]T_0} + \bar{A}_r\mathrm{e}^{\mathrm{i}[\bar{\omega}_j-\bar{\omega}_r]T_0}\right\} \\ & - 2\sum_{j=1}^{Q}\hat{F}_j\sum_{r=1}^{R} S_{nr}^{12}\left\{\mathrm{i}A_r\mathrm{e}^{\mathrm{i}[\bar{\omega}_j+\bar{\omega}_r]T_0} - \mathrm{i}\bar{A}_r\mathrm{e}^{\mathrm{i}[\bar{\omega}_j-\bar{\omega}_r]T_0}\right\} \\ & - 2\sum_{j=1}^{Q}\hat{F}_j\sum_{r=1}^{R} Q_{nr}^{11}\left\{A_r\mathrm{e}^{\mathrm{i}[\bar{\omega}_j+\bar{\omega}_r]T_0} + \bar{A}_r\mathrm{e}^{\mathrm{i}[\bar{\omega}_j-\bar{\omega}_r]T_0}\right\} \\ & - 2\sum_{j=1}^{Q}\hat{F}_j\sum_{r=1}^{R} Q_{nr}^{12}\left\{\mathrm{i}A_r\mathrm{e}^{\mathrm{i}[\bar{\omega}_j+\bar{\omega}_r]T_0} - \mathrm{i}\bar{A}_r\mathrm{e}^{\mathrm{i}[\bar{\omega}_j-\bar{\omega}_r]T_0}\right\} + \text{c.c.}, \end{aligned} \tag{58}$$

$$
\begin{aligned}
D_0\eta_{n1}+\bar{\omega}_n\varsigma_{n1} = & -\mathrm{i}D_1A_n\mathrm{e}^{\mathrm{i}\bar{\omega}_nT_0}\\
& -2\sum_{j=1}^{Q}\hat{F}_j\sum_{r=1}^{R}S_{nr}^{21}\left\{A_r\mathrm{e}^{\mathrm{i}[\bar{\omega}_j+\bar{\omega}_r]T_0}+\bar{A}_r\mathrm{e}^{\mathrm{i}[\bar{\omega}_j-\bar{\omega}_r]T_0}\right\}\\
& -2\sum_{j=1}^{Q}\hat{F}_j\sum_{r=1}^{R}S_{nr}^{22}\left\{\mathrm{i}A_r\mathrm{e}^{\mathrm{i}[\bar{\omega}_j+\bar{\omega}_r]T_0}-\mathrm{i}\bar{A}_r\mathrm{e}^{\mathrm{i}[\bar{\omega}_j-\bar{\omega}_r]T_0}\right\}\\
& -2\sum_{j=1}^{Q}\hat{F}_j\sum_{r=1}^{R}Q_{nr}^{21}\left\{A_r\mathrm{e}^{\mathrm{i}[\bar{\omega}_j+\bar{\omega}_r]T_0}+\bar{A}_r\mathrm{e}^{\mathrm{i}[\bar{\omega}_j-\bar{\omega}_r]T_0}\right\}\\
& -2\sum_{j=1}^{Q}\hat{F}_j\sum_{r=1}^{R}Q_{nr}^{22}\left\{\mathrm{i}A_r\mathrm{e}^{\mathrm{i}[\bar{\omega}_j+\bar{\omega}_r]T_0}-\mathrm{i}\bar{A}_r\mathrm{e}^{\mathrm{i}[\bar{\omega}_j-\bar{\omega}_r]T_0}\right\}+\text{c.c.}.
\end{aligned}
\tag{59}
$$

where $\bar{A}_r$ denotes the complex conjugate of A_r. This choice depends upon the resonant combinations of the frequencies; three cases are considered.

(i) Frequency $\bar{\omega}_j$ is far from $\bar{\omega}_p\pm\bar{\omega}_q$. The existence of the term $\mathrm{e}^{\mathrm{i}\bar{\omega}_nT_0}$ in the general solutions for Eqs. (58) and (59) may make finding the particular solutions difficult. After complexity of the calculation, the result indicates that the system will always be stable in this case.

(ii) Frequency $\bar{\omega}_j$ is near $\bar{\omega}_p+\bar{\omega}_q$. After complexity of the calculation, according to Mathieu theory, the system is stable if the solution of system is bounded [32]. If it is unbounded, the system is unstable. Therefore, the transition from stable to unstable corresponds to the unbinding of the solution. The transition curves separating stability from instability are given by

$$\bar{\omega}_j=\bar{\omega}_p+\bar{\omega}_q\pm2\varepsilon\sqrt{\Lambda_{pq}\bar{\Lambda}_{qp}}+O(\varepsilon^2) \tag{60}$$

where

$$\Lambda_{pq}=\sum_{j=1}^{Q}\hat{F}_j(-\mathrm{i}S_{pq}^{21}-S_{pq}^{22}-\mathrm{i}Q_{pq}^{21}-Q_{pq}^{22})-\sum_{j=1}^{Q}\hat{F}_j(-S_{pq}^{11}+\mathrm{i}S_{pq}^{12}-Q_{pq}^{11}+\mathrm{i}Q_{pq}^{12}), \tag{61}$$

$$\bar{\Lambda}_{qp}=\sum_{j=1}^{Q}\hat{F}_j(-\mathrm{i}S_{qp}^{21}-S_{qp}^{22}-\mathrm{i}Q_{qp}^{21}-Q_{qp}^{22})-\sum_{j=1}^{Q}\hat{F}_j(-S_{qp}^{11}+\mathrm{i}S_{qp}^{12}-Q_{qp}^{11}+\mathrm{i}Q_{qp}^{12}). \tag{62}$$

(iii) The frequency $\bar{\omega}_j$ is near $\bar{\omega}_p-\bar{\omega}_q$. Similarly, the transition curves for the combination of resonance for the different types can be determined from

$$\bar{\omega}_j=\bar{\omega}_p-\bar{\omega}_q\pm2\varepsilon\sqrt{\Lambda_{pq}\bar{\Lambda}_{qp}}+O(\varepsilon^2) \tag{63}$$

4. Analyses and discussion

The instability of a multimode spindle with realistically sized bearings is addressed and gas bearings are considered in this article. The dimensions $D=0.04\,\mathrm{m}$ and $L=0.2\,\mathrm{m}$ of a rotating

spindle are assumed. The bearing positions are $\bar{z}_1 = 0$ and $\bar{z}_2 = 1$. A spindle system braced by a gas bearing is important in engineering applications, especially those involving high-speed rotational machinery. For the above-mentioned spindle dimension, the data of gas bearing in this article is given as follows, viscosity $\mu = 1.833 \times 10^{-10}\,\mathrm{kg\,s/cm^2}$, the provided air pressure $49.225\,\mathrm{N/cm^2}$, applied air coefficient $\Gamma_s = 0.25$, the eccentric ratio $e = 0.3$, the number of pores $n = 8$, the pore diameter $d_g = 0.05\,\mathrm{mm}$ [24].

Fig. 3 plots the variation in the crack flexibility with various crack depth ratios. It was found that the crack flexibility increased as the crack depth is increased. Based on these results, the crack depth markedly affects the shaft stiffness. As a whole, these results and those from previous investigations are identical. The natural frequencies of a gas-bearing spindle system with and without cracks are shown in Fig. 4. At lower modes, the natural frequencies of a spindle with gas

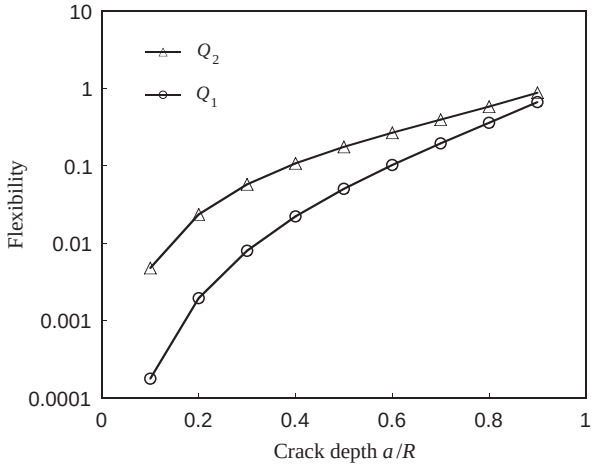

Fig. 3. The variations in the crack flexibility with various crack depth ratio.

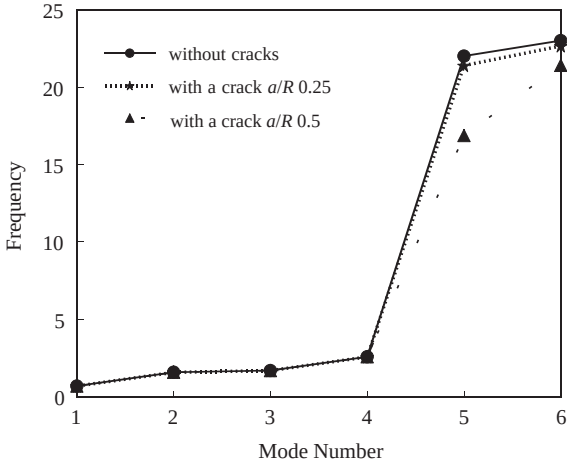

Fig. 4. The natural frequencies of a gas-bearing spindle with and without a crack ($\bar{\Omega} = 0.5$, $\bar{z}^* = 0.5$).

bearings change slightly whether there are cracks in the system or not. However, at higher modes, the natural frequencies of a spindle–bearing system markedly decrease when there is a crack in this spindle system. With gas bearings, the crack effect on the spindle system dynamics has greater influence at the higher mode than at the lower mode.

In actual high-speed rotating machinery applications, rotational speed cannot be maintained perfectly constant because of small perturbations during operation. Theoretically, at some specific rotational speed, the speed fluctuation may drive the system into a dynamically unstable condition. Thus, the dynamic instability of a spindle with bearings must be considered, especially for a gas-bearing spindle. For simplicity, the perturbation speed is assumed to be $\bar{f}(t) = 2\cos\bar{\omega}t$. Fig. 5 presents the dynamic instability of a rotating gas-bearing spindle with a crack. In this figure, the unstable regions are the dashed-line zones, near $2\bar{\omega}_1$, $\bar{\omega}_1 + \bar{\omega}_2$ and $\bar{\omega}_1 + \bar{\omega}_3$. The unstable regions near $2\bar{\omega}_1$ and $\bar{\omega}_1 + \bar{\omega}_3$ are gradually enlarged with the perturbation speed $\bar{f}(t)$, that is, the perturbation parameter ε, if the spindle–bearing system has a crack. In engineering applications, most investigators paid great attention to the lowest unstable zones in the system. Therefore, the variations in the lowest unstable zone of a spindle system with or without a crack are illustrated in Fig. 6. In Fig. 6(a), the lowest unstable zone, near $2\bar{\omega}_1$, is nearly independent of the perturbation, as with a gas-bearing spindle system without cracks. Fig. 6(b) shows the lowest unstable zone in this spindle system with a crack. The lowest unstable region near $2\bar{\omega}_1$ shifts to a lower frequency domain when a crack exists in the system. Note, the lowest unstable zone, near $2\bar{\omega}_1$, is enlarged as the gas-bearing–spindle system has a crack. It is clear that cracks not only alter the dynamics but also significantly change the instability of a gas-bearing–spindle system. Corresponding to Fig. 4, the higher mode unstable region is also considered in this article. The higher mode unstable region, the unstable region near $2\bar{\omega}_5$, of a system with or without a crack is shown in Fig. 7. In this figure, the unstable region near $2\bar{\omega}_5$ of a spindle system will become markedly enlarged if the system has a crack. Similarly, the crack affects the dynamics and the instability of a spindle system at the higher mode than at the lower mode.

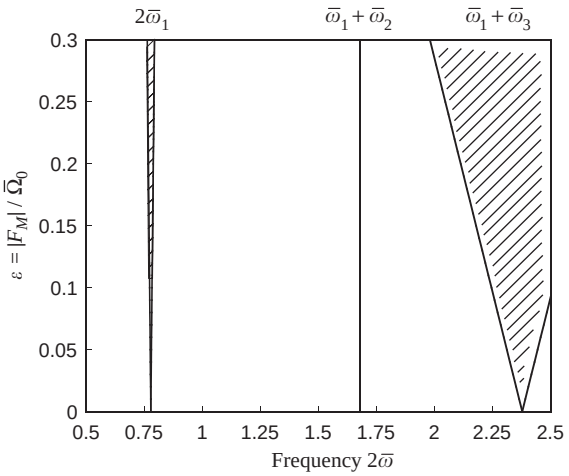

Fig. 5. The dynamic instability of a gas-bearing spindle with a crack ($\bar{\Omega} = 0.8$, $a/R = 0.6$, $\bar{z}^* = 0.5$).

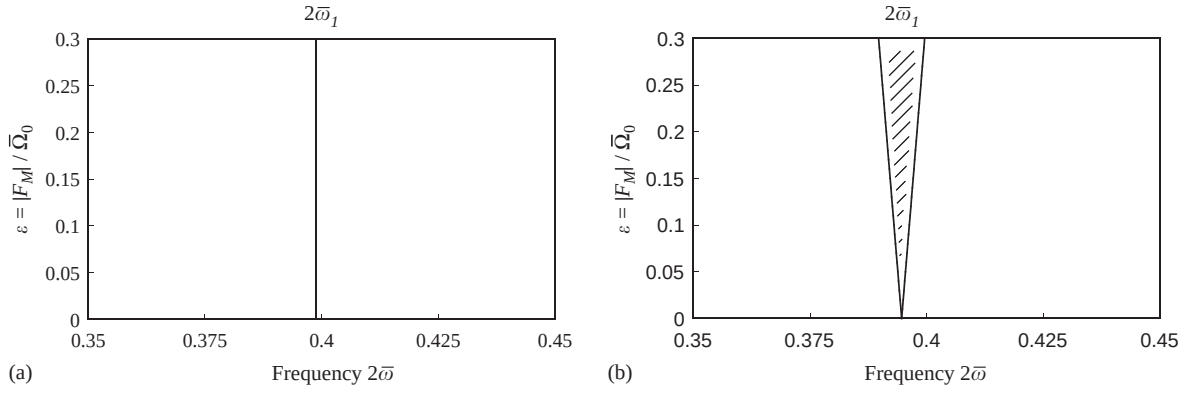

Fig. 6. The unstable region of a gas-bearing spindle with and without a crack (at the lowest mode, $\bar{\Omega} = 1$, $\bar{z}^* = 0.5$).

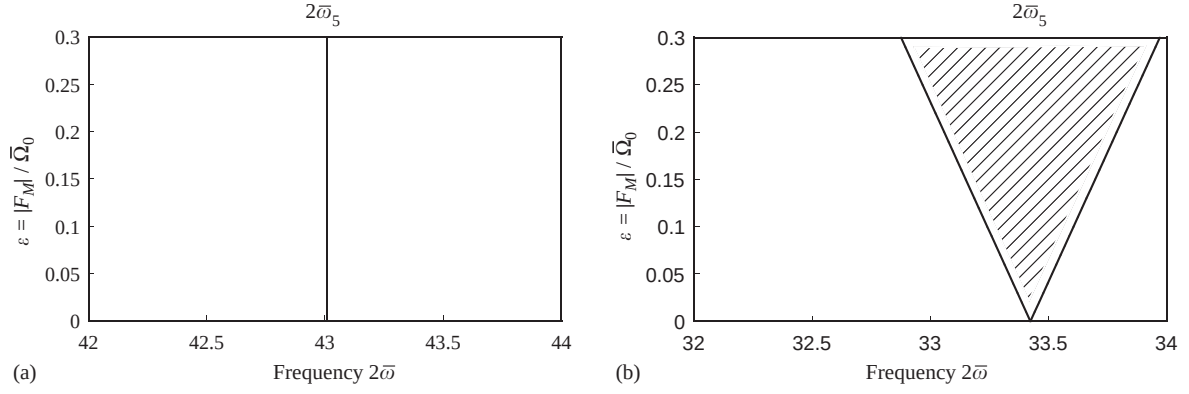

Fig. 7. The unstable region of a gas-bearing spindle with and without a crack (at higher mode, $\bar{\Omega} = 1$, $\bar{z}^* = 0.5$).

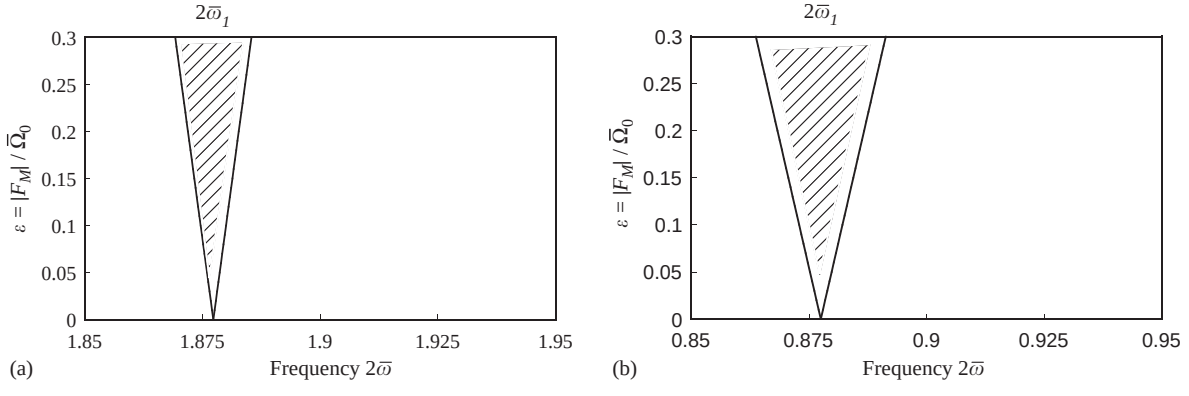

Fig. 8. The unstable region of a gas-bearing spindle with different rotational speeds ($\bar{z}^* = 0.5$, $a/R = 0.6$).

The effect of rotational speed on the dynamic instability of a rotating spindle system is also considered. Fig. 8 plots the variations in dynamic instability for a rotating spindle braced by gas bearings at various rotational speeds. The lowest unstable region near $2\bar{\omega}_1$ shifts to a lower frequency domain and is simultaneously enlarged. The results imply that varying the rotation speed may significantly affect the dynamic instability of a high-speed spindle with gas bearings. Fig. 9 illustrates the variations in the lowest natural frequency of a gas-bearing spindle with various amounts of provided air pressure. The results indicate that the lowest natural frequency of a spindle with gas bearings increases if the provided air pressure increases. It was found that the gas bearing stiffness is enhanced when the provided air pressure is increased. A variation in the dynamic instability of a gas-bearing spindle with various amounts of provided air pressure is plotted in Fig. 10. The lowest unstable region near $2\bar{\omega}_1$ shifts to a higher frequency domain as the spindle system is braced by stronger provided air pressure. Fig. 11 shows the variations in the dynamic instability of a spindle with various crack locations. As mentioned above, only the first

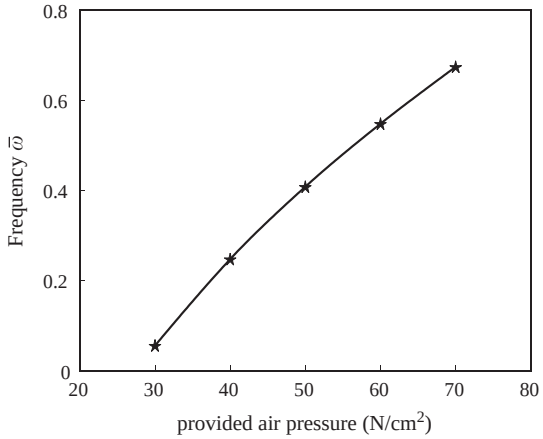

Fig. 9. The natural frequencies of a gas-bearing spindle with different provided air pressure ($\bar{\Omega} = 0.8$, $a/R = 0.5$, $\bar{z}^* = 0.5$).

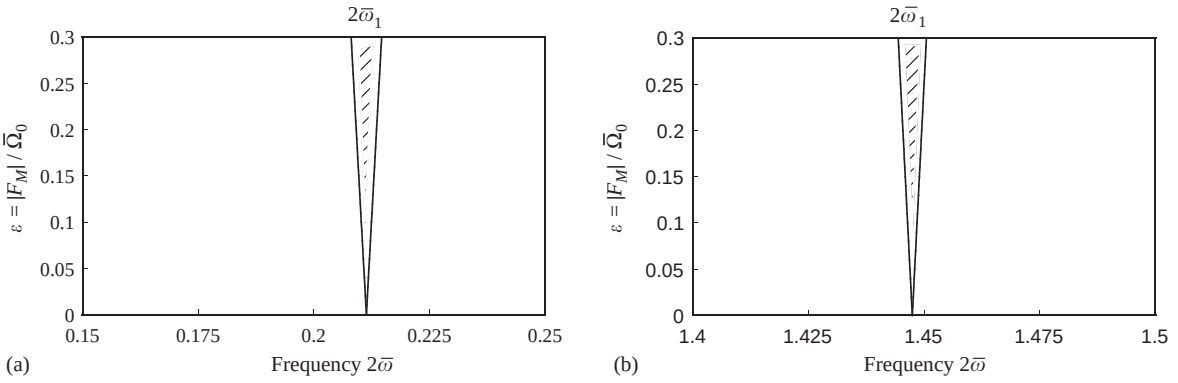

Fig. 10. The unstable region of a gas-bearing spindle with different provided air pressure ($\bar{\Omega} = 0.8$, $a/R = 0.5$, $\bar{z}^* = 0.5$).

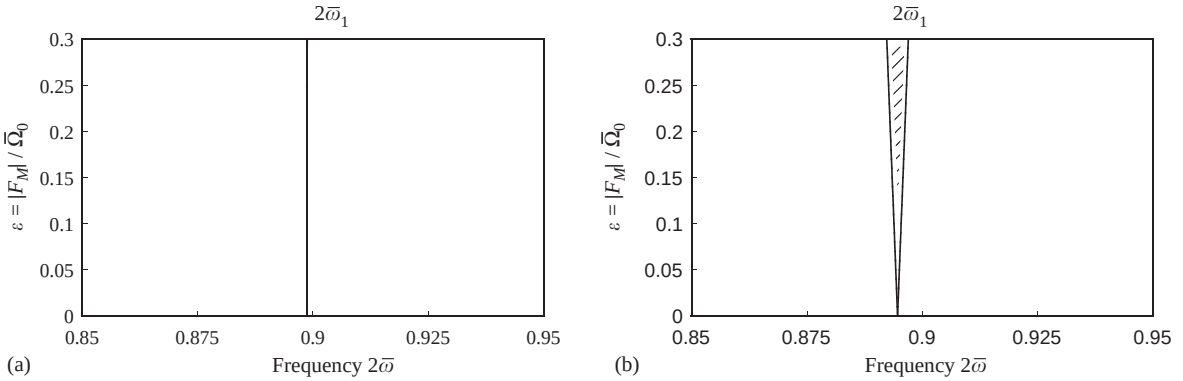

Fig. 11. The unstable region of a gas-bearing spindle with different location of the crack ($\bar{\Omega} = 0.75$, $a/R = 0.5$).

unstable zone was examined. When the crack is located at both ends, the lowest unstable zones are nearly the same as a system without a crack. The lowest unstable system region is the largest when the crack is located at the middle of the spindle.

5. Conclusions

The effect of cracks on the dynamic instability of a spindle supported by gas bearings was studied. The most significant observations in this study are summarized as follows:

1. With gas bearings, the natural frequencies of a spindle system will decrease as the crack depth increases, especially for higher mode frequencies.
2. The unstable zones of a spindle with gas bearings may broaden, as a crack exists in the spindle system. Numerical studies indicated that the cracks would markedly affect the dynamic instability of a spindle with gas bearings.
3. The effects of the provided air pressure and the crack location significantly change the dynamic instability of a spindle with gas bearings.
4. The rotational speed will dramatically affect the dynamic instability of a spindle with gas bearings.

Acknowledgements

The authors would like to thank the National Science Council, Taiwan, Republic of China, for financially supporting this research through Grant NSC 89-2622-E-327-001.

References

[1] S. Jayaram, S.G. Kapoo, R.E. DeVor, Analytical stability analysis of variable spindle speed machining, *Journal of Manufacturing Science and Engineering* 122 (2000) 391–397.

[2] R.G. Parker, P.J. Sathe, Free vibration and stability of a spinning disk–spindle system, *Journal of Vibration and Acoustics* 121 (1999) 391–396.
[3] M. Chinta, A.B. Palazzolo, Stability and bifurcation of rotor motion in a magnetic bearing, *Journal of Sound and Vibration* 214 (1998) 793–803.
[4] S.C. Huang, Y.M. Huang, S.M. Shieh, Vibration and stability of a rotating shaft containing a transverse crack, *Journal of Sound and Vibration* 162 (1993) 387–401.
[5] S.K. Bhaumik, R. Rangaraju, M.A. Venkataswamy, T.A. Bhaskaran, M.A. Parameswara, Fatigue fracture of crankshaft of an aircraft engine, *Engineering Failure Analysis* 9 (2002) 255–263.
[6] P.F. Rizos, N. Aspragathos, A.D. Dimarogonas, Identification of crack location and magnitude in a cantilever beam from the vibration mode, *Journal of Sound and Vibration* 138 (1990) 381–388.
[7] D. Broek, *Elementary Engineering Fracture Mechanics*, Martinus Nijhoff Publishers, Dordrecht, 1986.
[8] H. Tada, P. Paris, G. Irwin, *The Stress Analysis of Crack Handbook*, Del Research Corporation, Hellertown, PA, 1973.
[9] L. Chen, C. Chen, Vibration and stability of cracked thick rotating blade, *Computers & Structures* 28 (1988) 67–74.
[10] J.H. Kuang, B.W. Huang, Mode localization on a cracked bladed disk, *Journal of Engineering for Gas Turbine and Power* 121 (1999) 335–342.
[11] B.W. Huang, J.H. Kuang, The effect of local crack on the dynamic characteristics of a rotating grouped bladed disk, *IMechE Part C Journal of Mechanical Engineering Science* 216 (2002) 447–457.
[12] B. Grabowski, The vibrational behavior of a turbine rotor containing a transverse crack, *Journal of Mechanic Design* 102 (1980) 140–146.
[13] A.S. Sekhar, Effects of cracks on rotor system instability, *Mechanism and Machine Theory* 35 (2000) 1657–1674.
[14] N. Bachschmid, P. Pennacchi, E. Tanzi, A. Vania, Identification of transverse crack position and depth in rotor systems, *Meccanica* 35 (2000) 563–582.
[15] P.N. Saavedra, L.A. Cuitino, Vibration analysis of rotor for crack identification, *Journal of Vibration and Control* 8 (2002) 51–67.
[16] M.J. Goodwin, *Dynamics of Rotor-Bearing System*, Unwin Hyman, London, 1989.
[17] J.A. Brandon, K.J.H. Al-Shareef, On the applicability of modal and response representations in the dynamic analysis of machine tool spindle bearing systems, *IMechE Journal of Engineering Manufacture* 205 (1991) 139–145.
[18] B.R. Jorgensen, Y.C. Shin, Dynamics of spindle–bearing systems at high speeds including cutting load effects, *Journal of Manufacturing Science and Engineering* 120 (1998) 387–394.
[19] W.R. Wang, C.N. Chang, Dynamic analysis and design of a machine tool spindle–bearing system, *Journal of Vibration and Acoustics* 116 (1994) 280–285.
[20] R.G. Parker, C.J. Mote, Vibration and coupling phenomena in asymmetric disk–spindle systems, *Journal of Applied Mechanics* 63 (1996) 953–961.
[21] I.Y. Shen, Closed-form forced response of a damped, rotating, multiple disks/spindle system, *Journal of Applied Mechanics* 64 (1997) 343–352.
[22] G.L. Agrawal, The load capacity of shaped gas thrust bearing, in: *Proceedings of the Ninth International Gas Bearing Symposium*, Washington, DC, USA, 1986.
[23] P.L. Holster, J.A.H. Jacobs, Theoretical analysis and experimental verification on the static properties of externally pressurized air-bearing pads with load compensation, in: *Proceedings of the Ninth International Gas Bearing Symposium*, Washington, DC, USA, 1986.
[24] G.Y. Lie, *Gas Lubricated Bearings*, Hu-Han Press, Tainan, 1991 (in Chinese).
[25] K. Czolczynski, How to obtain stiffness and damping coefficients of gas bearings, *Wear* 201 (1996) 265–275.
[26] M.F. Chen, Y.P. Chen, C.D. Lin, Research on the arc type aerostatic bearing for a PCB drilling station, *Tribology International* 35 (2002) 235–243.
[27] Y. He, D. Guo, F. Chu, Using genetic algorithms to detect and configure shaft crack for rotor-bearing system, *Computer Methods in Applied Mechanics and Engineering* 190 (2001) 5895–5906.
[28] M.A. Mohiuddin, Y.A. Khulief, Dynamic response analysis of rotor-bearing systems with cracked shaft, *Journal of Mechanical Design* 124 (2002) 690–696.
[29] S. Prabhakar, A.S. Sekhar, A.R. Mohanty, Detection and monitoring of cracks in a rotor-bearing system using wavelet transforms, *Mechanical Systems and Signal Processing* 15 (2001) 447–450.

[30] A.D. Dimarogonas, S.A. Paipetis, *Analytical Methods in Rotor Dynamics*, Applied Science Publishers, New York, 1983.
[31] M. Krawczuk, W.M. Ostachowicz, Transverse natural vibrations of a cracked beam loaded with a constant axial force, *Journal of Vibration and Acoustics* 115 (1993) 524–528.
[32] A.H. Nayfey, D.T. Mook, Parametric excitations of linear systems having many degrees of freedom, *Journal of the Acoustical Society America* 62 (1977) 375–381.
[33] T.H. Young, G.T. Liou, Coriolis effect on the vibration of a cantilever plate with time-varying rotating speed, *Journal of Vibration and Acoustics* 114 (1992) 232–241.
[34] T.H. Young, Dynamic response of a pretwisted, tapered beam with non-constant rotating speed, *Journal of Sound and Vibration* 150 (1991) 435–446.
[35] C.L. Liao, B.W. Huang, Parametric resonance of a spinning pretwisted beam with time-dependent spinning rate, *Journal of Sound and Vibration* 180 (1995) 47–65.